

The complete NLO corrections to dijet hadroproduction

R. Frederix,^a S. Frixione,^b V. Hirschi,^c D. Pagani,^{a,d} H.-S. Shao,^e M. Zaro^{f,g}

^a*Physik Department T31, Technische Universität München, James-Frank-Str. 1, D-85748 Garching, Germany*

^b*INFN, Sezione di Genova, Via Dodecaneso 33, I-16146, Genoa, Italy*

^c*SLAC, National Accelerator Laboratory 2575 Sand Hill Road, Menlo Park, CA 94025-7090, USA*

^d*Centre for Cosmology, Particle Physics and Phenomenology (CP3), Université Catholique de Louvain, B-1348 Louvain-la-Neuve, Belgium*

^e*TH Department, CERN, CH-1211 Geneva 23, Switzerland*

^f*Sorbonne Universités, UPMC Univ. Paris 06, UMR 7589, LPTHE, F-75005, Paris, France*

^g*CNRS, UMR 7589, LPTHE, F-75005, Paris, France*

E-mail: rikkert.frederix@tum.de, Stefano.Frixione@cern.ch,
vahirsch@slac.stanford.edu, davide.pagani@tum.de,
huasheng.shao@cern.ch, zaro@lpthe.jussieu.fr

ABSTRACT: We study the production of jets in hadronic collisions, by computing all contributions proportional to $\alpha_S^n \alpha^m$, with $n+m=2$ and $n+m=3$. These correspond to leading and next-to-leading order results, respectively, for single-inclusive and dijet observables in a perturbative expansion that includes both QCD and electroweak effects. We discuss issues relevant to the definition of hadronic jets in the context of electroweak corrections, and present sample phenomenological predictions for the 13-TeV LHC. We find that both the leading and next-to-leading order contributions largely respect the relative hierarchy established by the respective coupling-constant combinations.

KEYWORDS: Hadronic collisions, NLO computations, Electroweak theory, Jets

Contents

1	Introduction	1
2	Calculation setup	2
3	Definition of jets	4
3.1	Photon-jet cross sections	7
4	Results	8
5	Conclusions	20
	References	24

1 Introduction

Jet production is a very common occurrence at high-energy hadron colliders; for example, at the 13-TeV LHC with an instantaneous luminosity of $\mathcal{L} = 10^{34} \text{ cm}^{-2}\text{s}^{-1}$, there are several tens of thousands events per second that contain at least one jet with transverse momentum larger than 100 GeV. Such an abundance allows experiments to carry out measurements affected by very small statistical uncertainties, and thus to probe all corners of the phase space in a multi-differential manner. At the same time, it constitutes a severe problem for new-physics searches characterised by jet final states, with the signal possibly swamped by Standard Model (SM) backgrounds. This also applies to the easiest of cases, that of a dijet signature (which is present in many beyond-the-SM scenarios, such as those that feature heavy vector bosons, excited quarks, axigluons, Randall-Sundrum gravitons, and so forth – see e.g. ref. [1] for a review of experimental searches that focus on the dijet-mass spectrum), whose peak structure can be diluted by QCD effects or be difficult to study if at the border of the kinematically accessible region. A well known example of the latter situation was the high- p_T excess reported by CDF [2] in inclusive jet events, that triggered a lot of interest owing to its being a possible evidence of quark compositeness, but that was ultimately entirely due to an SM effect. In particular, the PDFs used for computing the SM predictions to which the data had been compared were insufficiently constrained in the x region that dominated high- p_T jet production, and the uncertainties associated with their determination were unknown.

The case of the large transverse momentum excess at CDF typifies the necessity of computing jet cross sections at the highest possible accuracy in the SM. The largest of such cross sections is the dijet one (which also gives the dominant contribution to single-inclusive rates); we shall exclusively deal with it in this paper. Next-to-leading order (NLO) QCD

results for inclusive and two-jet distributions have been available since the early 1990’s [3–6]. The first complete next-to-NLO (NNLO) QCD predictions have appeared only very recently [7]. As a rule of thumb based on the values of the respective coupling constants, NNLO QCD effects ($\mathcal{O}(\alpha_s^4)$) have the same numerical impact as the so-called NLO ones in the electroweak (EW) theory ($\mathcal{O}(\alpha_s^2\alpha)$). Partial pure-weak contributions to the latter had been computed in refs. [8, 9], and the complete weak results published in ref. [10]. The rationale for ignoring the NLO EW corrections of electromagnetic origin, which to the best of our knowledge have not been calculated so far, is the possible enhancement of weak contributions due to the growth of logarithmic terms of Sudakov origin in certain regions of the phase space associated with large scales [11–14], in particular at high transverse momenta. Incidentally, such Sudakov effects can also be responsible for large violations of the natural hierarchy of QCD and EW corrections, with NLO EW ones becoming significantly larger than their NNLO QCD counterparts and competitive with the NLO QCD results.

Motivated by the previous considerations, in this paper we present the computation of *all* the leading and next-to-leading order contributions to the dijet cross section in a mixed QCD-EW coupling scenario. In other words, we compute all the terms in the perturbative series that factorise the coupling-constant combinations $\alpha_s^n\alpha^m$, with $n+m=2$ (leading order, LO) and $n+m=3$ (NLO). Thus, we calculate here for the first time the $\mathcal{O}(\alpha_s^2\alpha)$ electromagnetic contribution, and the two NLO terms of $\mathcal{O}(\alpha_s\alpha^2)$ and $\mathcal{O}(\alpha^3)$. Our computations are carried out in the MADGRAPH5_AMC@NLO framework [15] (MG5_AMC henceforth), and are completely automated; this work therefore constitutes a further step in the validation of the MG5_AMC code, in a case that requires the subtraction of QED infrared singularities which is significantly more involved than that studied in ref. [16]. We also take the opportunity to discuss issues that arise when one defines jets in the presence of final-state photon and leptons.

This paper is organised as follows. In sect. 2 we outline the contents of our computation and the general features of the framework in which it is performed. The problem of the definition of jets in the context of higher-order EW calculations is discussed in sect. 3. Phenomenological results for the LHC Run II are given in sect. 4. Finally, we present our conclusions in sect. 5.

2 Calculation setup

A generic observable in two-jet hadroproduction can be written as follows:

$$\begin{aligned}\Sigma_{jj}^{(\text{LO})}(\alpha_s, \alpha) &= \alpha_s^2 \Sigma_{2,0} + \alpha_s \alpha \Sigma_{2,1} + \alpha^2 \Sigma_{2,2} \\ &\equiv \Sigma_{\text{LO}_1} + \Sigma_{\text{LO}_2} + \Sigma_{\text{LO}_3},\end{aligned}\tag{2.1}$$

$$\begin{aligned}\Sigma_{jj}^{(\text{NLO})}(\alpha_s, \alpha) &= \alpha_s^3 \Sigma_{3,0} + \alpha_s^2 \alpha \Sigma_{3,1} + \alpha_s \alpha^2 \Sigma_{3,2} + \alpha^3 \Sigma_{3,3} \\ &\equiv \Sigma_{\text{NLO}_1} + \Sigma_{\text{NLO}_2} + \Sigma_{\text{NLO}_3} + \Sigma_{\text{NLO}_4},\end{aligned}\tag{2.2}$$

at the LO and NLO respectively. The notation we adopt throughout this paper is fully analogous to that of refs. [15–17]. We refer the reader, in particular, to ref. [17] for a detailed discussion on the physical meaning of the terms that appear in eqs. (2.1) and (2.2), and

the relevant terminology; we limit ourselves to recalling here that what is conventionally denoted by NLO QCD and NLO EW corrections can be identified with Σ_{NLO_1} and Σ_{NLO_2} , respectively.

In our computation, $\Sigma_{jj}^{(\text{LO})}$ receives contributions from all Feynman diagrams relevant to tree-level four-point Green functions with external massless SM particles – namely, light quarks (including bottoms, since we work with five light flavours), gluons, photons, and leptons¹. As far as $\Sigma_{jj}^{(\text{NLO})}$ is concerned, all one-loop four-point and tree-level five-point functions with massless external legs contribute. Note that this implies that while both real and virtual photons enter NLO corrections, W^\pm 's and Z 's only appear as internal particles. Thus, what has been called HBR (for Heavy Boson Radiation) in refs. [16, 17], that is the contribution from tree-level diagrams that correspond to the real emission of a W^\pm or a Z (and, in principle, one might consider top-quark emissions, too) from a Born-level configuration, is not included in our results (incidentally, this is also the reason why in the present case $\Sigma_{\text{NLO EW}} \equiv \Sigma_{\text{NLO}_2}$). In fact, in order to consider HBR cross sections, one would need either to possibly cluster a heavy vector boson together with other massless particles when reconstructing jets (an option which is not appealing from a physics viewpoint, given the procedure followed by experiments), or to first decay any W^\pm and Z into a pair of quarks or leptons. Having said that, we point out that MG5_AMC can be used to simulate HBR contributions to dijet observables, and that the corresponding calculations are fully independent of those performed here.

All of the computations of the matrix elements mentioned above, the renormalisation procedure, and the subtraction of the real-emission infrared singularities (IR) are handled automatically by MG5_AMC (with a still-private version of the code). We remind the reader that MG5_AMC makes use of the FKS method [18, 19] (automated in the module MADFKS [20, 21]) for dealing with IR singularities. The computations of one-loop amplitudes are carried out by switching dynamically between two integral-reduction techniques, OPP [22] or Laurent-series expansion [23], and TIR [24–26]. These have been automated in the module MADLOOP [27], which in turn exploits CUTTOOLS [28], NINJA [29, 30], or IREGI [31], together with an in-house implementation of the OPENLOOPS optimisation [32]. Two remarks are in order here. Firstly, there is no element in the MG5_AMC code that has been customised to compute dijet observables, in keeping with the general strategy that underpins the code. Secondly, although the papers cited above mostly treat explicitly the case of QCD corrections, MG5_AMC has been constructed for being capable to handle other theories as well. For what concerns the subtraction of real-emission singularities, the QED case descends from the QCD one, with the most significant complications in the context of automation due to bookkeeping (which understands the necessity of retaining independent control of the various $\Sigma_{k,q}$ terms). The underlying strategy has been outlined in sect. 2.4.1 of ref. [15]; the necessary extensions to the code were chiefly carried out for the work of ref. [16], and further validated for the present paper. As far as one-loop computations are concerned, MADLOOP has been completely overhauled in ref. [15] (see in particular sects. 2.4.2 and 4.3 there), and it is since then that it is able to evaluate virtual

¹The reasons for this choice will be discussed in sect. 3.

amplitudes in theories other than QCD.

Finally, we point out that our simulations are entirely based on a Monte Carlo integration of the short-distance subtracted cross sections, that results in (weighted) events and their associated counterevents. In particular, we do not use any factorised formulae for the one-loop EW logarithmic corrections (see e.g. ref. [13]).

3 Definition of jets

The prescription for the computation of a jet cross section, possibly in association with other objects, is unambiguous in perturbative QCD: jets are composed of massless coloured particles (quarks and gluons), and this determines the nature of parton-level processes. Things become more complicated as soon as one considers the first subleading higher-order correction, i.e. the electromagnetic one at the NLO. Among other things, this entails the contribution of diagrams with an extra (w.r.t. the underlying Born configuration) real photon in the final state. In order to have an IR-finite cross section, such a photon must be recombined (at least in a suitable subset of the phase space) with nearby QCD partons to form a jet. However, this raises an issue when the jet is made of a photon and a gluon: IR safety demands (consider the soft-gluon limit) that there be an associated Born configuration in which a jet coincides with a photon. In other words, Born-level amplitudes must feature both QCD partons and photons (which in turn implies that one cannot limit oneself to considering only the leading, pure-QCD, Born contribution).

This does not really pose any problem: one must simply enlarge the set of particles that can form jets at the level of short-distance cross sections (both at the leading and at higher orders), and include photons on top of light quarks and gluons; the resulting objects are called *democratic jets*². The fact that a jet might be predominantly a non-hadronic quantity is not surprising in a realistic experimental environment; for example, in certain LHC analyses a jet is a spray of collimated particles with up to 99% of its energy of electromagnetic origin, of which up to 90% can be carried by a single photon (see e.g. refs. [34–46] for a list of recent ATLAS and CMS papers approved as publications in the context of jet physics). Having said that, fixed-order perturbation theory is somehow pathological, precisely because a jet can coincide with a photon. Although, as we shall show later, this situation is numerically unimportant, it has motivated the introduction of procedures with the aim of getting rid of jets whose energy content is dominated by a photon – in this paper, we shall call such objects *photon jets*. Recent examples can be found in refs. [47–50], that deal with NLO EW corrections to vector boson production in association with jets. The common feature of these procedures is the use of the photon energy (or of a related quantity, such as the transverse momentum), which is necessary to define the photon hardness, and thus its relative contribution to that of the jet the photon belongs to.

²Starting from the third-leading NLO corrections (that scale like $(\alpha/\alpha_S)^2$ w.r.t. the leading, pure-QCD, ones) it is necessary to include massless leptons as well in the jet-clustering procedure. As far as we know, the term “democratic” applied to jets in a similar context has been used for the first time in ref. [33].

Unfortunately, the photon energy is an ill-defined perturbative concept, starting from the third-leading NLO correction (i.e. Σ_{NLO_3} in the case of dijet production). This can be easily seen by considering a Born-level diagram with a final-state photon, and the real-emission diagram obtained from the former by means of a $\gamma \rightarrow q\bar{q}$ splitting: by taking the $q \parallel \bar{q}$ limit, one sees that the photon energy is not an IR-safe quantity.

In order to use photon degrees of freedom in an IR-safe way, the photon must be a physical final-state object (in other words, “taggable” or “observable”). For this to happen, the following rule must be obeyed:

- Photons can be considered as observable objects only if emerging from a fragmentation process. A photon that appears in a Feynman diagram has not been fragmented, and thus cannot be tagged.

A taggable photon is quite analogous to e.g. a pion, which is described in perturbative QCD by means of a (non-perturbative) fragmentation process. As such, we shall have fragmentation functions that account for the long-distance process:

$$D_\gamma^{(i)}(z) : \quad i \longrightarrow \gamma, \quad (3.1)$$

where i is any massless particle that can fragment into a photon, and z the fraction of the longitudinal momentum of i carried by the photon. Thus, the particle i may be itself a photon, which is the most significant difference between the photon and the pion cases (since no pion can appear at the short-distance level). In particular, owing to the elementary nature of the photon, one will necessarily have [51]:

$$D_\gamma^{(\gamma)}(z) = (A + B\alpha + \dots) \delta(1 - z) + \Delta D_\gamma^{(\gamma)}(z), \quad (3.2)$$

with $\Delta D_\gamma^{(\gamma)}(z)$ a regular function at $z \rightarrow 1$. We point out that the $\mathcal{O}(\alpha^0) \delta(1 - z)$ term in eq. (3.2) is all one needs in the context of QCD computations that feature final-state photons³: in that case, the difference between taggable photons and short-distance photons is irrelevant (and indeed it is not necessary to introduce it). We also remark that it is perfectly acceptable to have a process with both taggable and short-distance photons in the final state; the degrees of freedom of the latter must be integrated over (as e.g. in a jet-finding algorithm), while this is not necessary (but still possible) for the former ones.

The scheme outlined above allows one to define a photon jet regardless of the perturbative order in α_s and α one is working at: for example, a photon jet is any jet that contains a taggable photon with energy E_γ such that $E_\gamma \geq z_{cut} E_j$, with E_j the jet energy and z_{cut} a pre-defined constant. However, in the context of a jet analysis what one is really interested in is a “hadronic” jet, i.e. a jet in which the content of EM energy is smaller, not larger, than a given threshold (we shall call these jets *anti-tagged jets* in this paper). This poses two problems. Firstly, a photon can be anti-tagged not only if $E_\gamma < z_{cut} E_j$, but also if it simply escapes detection (which, for a fixed-order theoretical calculation, is the case where the jet is made of quarks and gluons only, i.e. one in which there is no photon).

³Such a term corresponds to what is usually called the direct contribution in pQCD calculations.

Secondly, the anti-tagging condition creates a practical problem, because fragmentation functions can only be measured (if at all) for sufficiently large z 's.

A possible solution to these problems employs again the idea of photon jet. The starting point is the following identity (which is the hadron-parton-duality unitary condition):

$$i = \sum_h D_h^{(i)}(z) + \dots = \sum_{h \neq \gamma} D_h^{(i)}(z) + D_\gamma^{(i)}(z) + \dots \quad (3.3)$$

where the dots on the r.h.s. generically denote power-suppressed terms. In words: parton i fragments into any “hadrons”, which will be eventually clustered into a jet (note that parton i can be dressed by the perturbative radiation of other massless particles – these are understood in the notation of eq. (3.3)). In the rightmost side of eq. (3.3), the sum over parton-to-hadron fragmentation functions is split into the sum of a term that features all hadrons different from the photon, and of a parton-to-photon term. By neglecting the power-suppressed terms we re-write eq. (3.3) as follows:

$$i = \sum_{h \neq \gamma} D_h^{(i)}(z) + D_\gamma^{(i)}(z)\Theta(z_{cut} - z) + D_\gamma^{(i)}(z)\Theta(z - z_{cut}), \quad (3.4)$$

i.e. we introduce tagging and anti-tagging conditions, which we can do because the photon emerges from a fragmentation process, and thus is taggable. Thence:

$$\sum_{h \neq \gamma} D_h^{(i)}(z) + D_\gamma^{(i)}(z)\Theta(z_{cut} - z) = i - D_\gamma^{(i)}(z)\Theta(z - z_{cut}). \quad (3.5)$$

The l.h.s. of eq. (3.5) is what we want: the anti-tag jet contribution. Unfortunately, neither of the terms that appear there can be reliably computed (for all z 's). Conversely, the r.h.s. of that equation is just fine: the two terms there correspond to the fully-democratic jet cross section and to the photon-tagged one. If eq. (3.5) is iterated over all possible final-state partons, one ends up by *defining* in a natural manner the anti-tag jet cross section as the democratic cross section, minus all tagged-photon cross sections, with the number of photons ranging from one to the maximum number of jets compatible with the perturbative order considered. In formulae, this can be expressed as follows:

$$d\sigma_{X;nj}^{(\text{antitag})} = d\sigma_{X;nj}^{(\text{dem})} - \sum_{k=1}^n d\sigma_{X+k\gamma;nj}. \quad (3.6)$$

with X any set of objects that have to be found in the final state on top of n jets (importantly, taggable photons may appear in such a set). The first term on the r.h.s. of eq. (3.6) is the democratic jet cross section; no taggable photons are present, except those possibly in X . Each of the n cross sections that appear in the second term on the r.h.s. of eq. (3.6) is constructed by using the same short-distance processes as those that contribute to the first term, and by fragmenting k final-state quarks, gluons, and photons in all possible ways; n jets are finally reconstructed. All $n + 1$ terms on the r.h.s. of eq. (3.6) are finite and IR safe, and can be computed independently of each other in perturbation theory.

What has been done so far for photons can essentially be repeated in the case of massless leptons. The main difference is that a fermion line cannot be made to disappear

by splitting, and this implies that there is a way to tag a lepton that is not viable in the case of photons. Still, IR safety requires that such a tagging is performed on an object which is not the (short-distance) lepton itself, but its dressed version: this is nothing but a jet, typically constructed with a small aperture, that contains one lepton and whatever extra radiation surrounds it. Alternatively, one can follow the same procedure as for photons, namely introduce parton-to-lepton fragmentation functions. Either way, one arrives at the idea of taggable leptons, which can be employed to define lepton jets; the anti-tag jet cross section in the l.h.s. of eq. (3.6) is then defined by inserting on the r.h.s. subtraction terms relevant to the lepton-jet cross sections⁴.

The procedure outlined so far puts QCD and QED on a rather similar footing. In particular, this implies that as far as EW corrections are concerned all computations can be conveniently performed in an $\overline{\text{MS}}$ -like scheme (such as the G_μ or $\alpha(m_Z)$ ones). We point out that this procedure naturally leads to the prescription usually adopted in NLO EW computations (see e.g. ref. [53]) that associates a factor $\alpha(0)$ to each external (short-distance) photon: such a factor results from the RG evolution of the photon-to-photon fragmentation function, whose $\delta(1-z)$ term acquires an overall factor $\alpha(0)/\alpha(Q)$ [51].

3.1 Photon-jet cross sections

We now return to eq. (3.6) in order to define the photon-jet cross sections that appear in the second term on the r.h.s. of that equation, for the case of dijet hadroproduction we are interested in. As was discussed above, a construction valid for all the $\alpha_s^n \alpha^m$ combinations necessarily entails the use of fragmentation functions, whose knowledge is presently far from being satisfactory (bar perhaps for the quark-to-photon one).

Therefore, we have to adopt a pragmatic solution; this amounts to defining the photon-jet cross sections only for those $\mathcal{O}(\alpha_s^n \alpha^m)$ terms for which the introduction of a fragmentation function can be bypassed; for the other terms, the photon-jet cross sections will be set equal to zero, and thus our anti-tag dijet cross section will coincide with the democratic one⁵. We do this in the following way. The photon-jet cross sections are defined by using the isolated-photon cross sections for one and two photons, constructed identically to what one usually does in perturbative QCD, and whose final states are suitably clustered into jets (as we shall specify later). This implies that the relevant perturbative orders are the following:

$$1\gamma : \mathcal{O}(\alpha_s \alpha + \alpha_s^2 \alpha) \equiv \Sigma_{\text{LO}_2} + \Sigma_{\text{NLO}_2}, \quad (3.7)$$

$$2\gamma : \mathcal{O}(\alpha^2 + \alpha_s \alpha^2) \equiv \Sigma_{\text{LO}_3} + \Sigma_{\text{NLO}_3}, \quad (3.8)$$

for the one- and two-isolated-photon cross sections respectively. This is implicitly equivalent to setting the photon-to-photon fragmentation function equal to $\delta(1-z)$, i.e. to neglecting the contribution to it due to higher-order QED effects. The cross sections that

⁴The use of the physical lepton masses leads to alternative approaches (see e.g. ref. [52]). These typically feature large-logarithmic terms, that expose their IR sensitivity and necessitate a careful treatment; we believe that they are best avoided in the context of jet analyses and lepton-jet rejection.

⁵We always cluster leptons democratically, which is fully justified by the fact that their contributions are very subleading, and numerically completely negligible.

correspond to eqs. (3.7) and (3.8) could still depend on quark-to-photon and gluon-to-photon fragmentation functions; in order to avoid this, we choose to work with the smooth isolation prescription of ref. [54], which sets their contributions identically equal to zero. More in details, we have implemented the following procedure:

1. find jets democratically;
2. find isolated photons; they are defined following ref. [54] (using transverse momenta), with the same cone aperture as for jets, and with $n_\gamma = \epsilon_\gamma = 1$;
3. loop over those photons: if a photon belongs to a jet, and it carries more than 90% of the p_T of that jet, then flag the jet as a candidate photon jet;
4. candidate photon jets are considered as proper photon jets if and only if:
 - there is exactly one isolated photon, and one computes either Σ_{LO_2} or Σ_{NLO_2} ;
 - there are exactly two isolated photons, and one computes either Σ_{LO_3} or Σ_{NLO_3} ;
5. each photon jet gives an entry to the histograms relevant to single-inclusive observables. For dijet correlations, there is an histogram entry for each pair of jets, at least one of which is a photon jet⁶.

There are many possible variants to items 1–5 above, but we believe that all those that are consistent with the general ideas outlined before will give very similar numerical results. The most important thing to bear in mind is that, regardless of the specific choices made for the isolation procedure, one is guaranteed to get rid of those configurations where a photon jet coincides with a photon, which is the semi-pathological situation, peculiar of fixed-order calculations, that one typically would like to avoid.

We point out that, with the choices made here, each photon jet will coincide with a democratic jet (while the opposite is obviously not true). Therefore, item 5 implies a local and exact cancellation of the photon-jet contributions, if all the computations relevant to the cross sections on the r.h.s. of eq. (3.6) are performed simultaneously (i.e. during the same run), which is what we do. This not only improves the numerical stability of the results, but also resembles very closely any possible experimental procedure that would reject jets with too high a content of EM energy.

4 Results

We now turn to presenting our predictions for a variety of single-inclusive and dijet observables that result from pp collisions at a center of mass energy of 13 TeV (LHC Run II). We refer the reader to eqs. (2.1) and (2.2) for the definitions of the LO (Σ_{LO_i} , $i = 1, 2, 3$) and NLO (Σ_{NLO_i} , $i = 1, 2, 3, 4$) contributions to the cross section, respectively; here, we shall show different linear combinations of these quantities. Jets are defined by means of the k_T algorithm [55] with $D = 0.7$, and reconstructed with FASTJET [56]; as a default, we present results relevant to democratic jets, but also explicitly assess the effect of removing photon

⁶We point out that dijet correlations can be constructed by using a subset of all possible two-jet pairings, and we choose in sect. 4 to consider only observables defined by means of the two hardest jets.

jets, as discussed in sect. 3. For all of the observables considered here the contribution of forward jets is discarded, by imposing the constraint:

$$|y| < 2.8. \quad (4.1)$$

We work in the five-flavour scheme (5FS) where all quarks, including the b , are massless; electrons, muons, and taus, collectively called leptons, are massless as well, while the vector boson masses and widths have been set as follows:

$$m_W = 80.419 \text{ GeV}, \quad m_Z = 91.188 \text{ GeV}, \quad (4.2)$$

$$\Gamma_W = 2.09291 \text{ GeV}, \quad \Gamma_Z = 2.50479 \text{ GeV}. \quad (4.3)$$

The CKM matrix is taken to be diagonal, and the complex-mass scheme [57, 58] is employed throughout. The PDFs are those of the NNPDF2.3QED set [59], extracted from LHAPDF6 [60] with number 244600; these are associated with

$$\alpha_s(m_Z) = 0.118. \quad (4.4)$$

We work in the G_μ EW scheme, where:

$$G_\mu = 1.16639 \cdot 10^{-5} \quad \longrightarrow \quad \frac{1}{\alpha} = 132.507. \quad (4.5)$$

The central values of the renormalisation (μ_R) and factorisation (μ_F) scales are both equal to:

$$\mu_0 = \frac{H_T}{2} \equiv \frac{1}{2} \sum_i p_T(i), \quad (4.6)$$

where the sum runs over all final-state particles. The theoretical uncertainties due to the μ_R and μ_F dependencies have been evaluated by varying these scales independently in the range:

$$\frac{1}{2}\mu_0 \leq \mu_R, \mu_F \leq 2\mu_0, \quad (4.7)$$

and by taking the envelope of the resulting predictions. The scale dependence of α is ignored, and the systematics associated with the variations in eq. (4.7) is evaluated by means of the exact reweighting technique introduced in ref. [61]. Reweighting is also employed for the computation of PDF uncertainties, with individual weights combined according to the NNPDF methodology [62]. We report the 68% CL symmetric interval (that is the one that contains only 68 replicas out of a total of a hundred; this is done in order to avoid the problem of outliers, which is severe in this case owing to the photon PDF [59]). Finally, we note that the NNPDF2.3 set adopts a variable-flavour-number scheme. For scales larger than the top mass, this scheme is equivalent to the six-flavour one (6FS). Since the hard matrix elements are evaluated in the 5FS, the impact of the sixth flavour has to be removed from the running of α_s and from the DGLAP evolution of the PDFs. This corresponds to adding to the NLO 6FS-PDF cross section the following quantity:

$$\alpha_s \frac{T_F}{3\pi} \sum_{i,k} \left[n_g^{(i,k)} \log \left(\frac{\mu_F^2}{m_t^2} \right) \Theta(\mu_F - m_t) - b^{(i,k)} \log \left(\frac{\mu_R^2}{m_t^2} \right) \Theta(\mu_R - m_t) \right] \Sigma_{\text{LO}_{ik}}. \quad (4.8)$$

Here, $n_g^{(i,k)}$ and $b^{(i,k)}$ are the number of initial-state gluons and the power of α_S in $\Sigma_{\text{LO}_{ik}}$, respectively, with k numbering the individual partonic channels that contribute to Σ_{LO_i} . The interested reader can find more details in ref. [63] or in sect. IV.2.2 of ref. [64].

In order to determine which transverse-momentum cuts are sensible in an NLO computation, we follow the procedure of ref. [65] and present in fig. 1 the total dijet cross section as a function of Δ , according to the following definition:

$$\sigma(\Delta) = \sigma\left(p_T^{(j_1)} \geq 60 \text{ GeV} + \Delta, p_T^{(j_2)} \geq 60 \text{ GeV}\right), \quad (4.9)$$

with $p_T^{(j_1)}$ and $p_T^{(j_2)}$ the transverse momentum of the hardest and second-hardest jet, respectively. In other words, Δ measures the asymmetry between the p_T cuts imposed on the two hardest jets, having assumed the transverse momentum of the second-hardest jet to be larger than 60 GeV. Such a value is arbitrary, and is chosen as typical of LHC jet analyses; we point out that its impact on the pattern of the dijet cross section dependence upon Δ is negligible (within a reasonable range). There are five curves in the main frame of fig. 1.

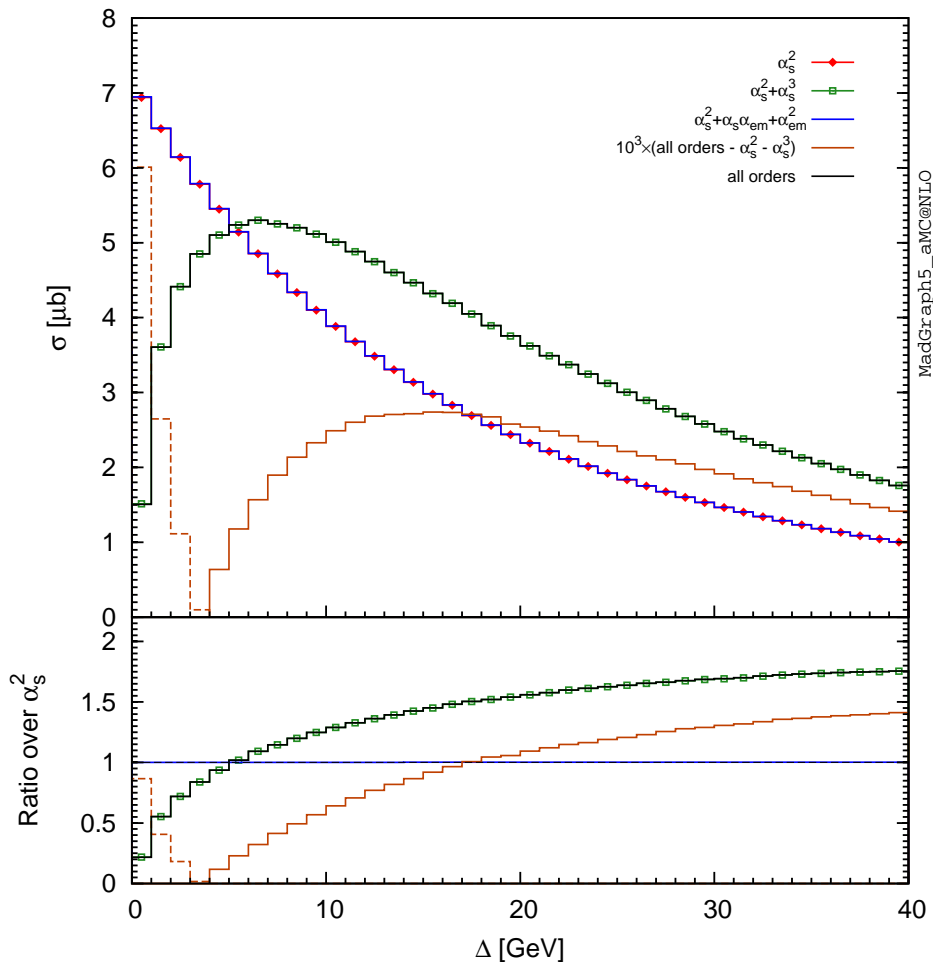


Figure 1. Total dijet cross section as a function of Δ , according to the definition given in eq. (4.9).

The red histogram overlaid with full diamonds represents the Σ_{LO_1} contribution, while the blue one corresponds to the sum of all of the LO contributions, $\Sigma_{jj}^{(\text{LO})}$. The green histogram overlaid with open boxes is the sum $\Sigma_{\text{LO}_1} + \Sigma_{\text{NLO}_1}$, i.e. of the leading terms (pure QCD) at the LO and NLO; the black histogram is the sum of all of the LO and NLO contribution, $\Sigma_{jj}^{(\text{LO})} + \Sigma_{jj}^{(\text{NLO})}$, and is denoted by “all orders”. Finally, the brown curve represents the sum of all LO and NLO contributions, bar the pure QCD ones (Σ_{LO_1} and Σ_{NLO_1}); in order for it to fit into the frame of the figure, this histogram has been rescaled by a factor of 10^3 . In the region where the latter curve is displayed with a dashed pattern, the cross section is negative, and thus what is represented is its absolute value; this convention will be used throughout this section. The lower panel in fig. 1 presents the ratios of the results shown in the main frame, over the Σ_{LO_1} prediction.

As is explained in detail in ref. [65], the dijet cross section behaves in a pathological manner for small Δ values at the NLO, owing to the presence of large $\log \Delta$ terms. Given the definition in eq. (4.9), one would expect a monotonically increasing rate for $\Delta \rightarrow 0$. This is indeed the behaviour of the LO results (red-with-diamonds and blue histograms), while the NLO ones actually decrease as $\Delta = 0$ is approached. Figure 1 therefore helps decide which value of Δ is appropriate in order to carry out sensible NLO computations. Inspection of the plot suggests to set $\Delta \gtrsim 20$ GeV – for such values, the three NLO predictions are still monotonically growing. In order to be definite, we shall thus impose

$$p_T^{(j_1)} \geq 80 \text{ GeV}, \quad p_T^{(j_2)} \geq 60 \text{ GeV} \quad (4.10)$$

in our simulations for dijet correlations, while for single-inclusive distributions we impose

$$p_T^{(j)} \geq 60 \text{ GeV}. \quad (4.11)$$

There are a couple of further observations relevant to fig. 1. Firstly, the full LO and NLO results (blue and black histograms, respectively) are extremely close (but not identical, although that is hard to see directly from the plot) to their leading, pure-QCD, counterparts (red-with-diamonds and green-with-boxes histograms, respectively). This is the well-known fact that EW contributions are negligible as far as dijet rates are concerned, their effects being manifest only in certain phase-space regions characterised by large scales and that contribute little to total cross sections. Secondly, it appears that the impact of $\log \Delta$ terms is larger when the pure-QCD contributions are not included (the peak of the brown histogram occurs at a much larger Δ value than that relevant to the two other NLO results). This suggests that a conservative choice of Δ (similar to or even more stringent than that of eq. (4.10)) is recommended where EW effects are particularly prominent.

We now turn our attention to differential observables. We shall present six of them in figs. 2–14, with two figures for each observable (plus one relevant to the direct comparison of p_T results in different rapidity ranges, fig. 10). The patterns in the layout of the plots are the same for all of the observables; thus, we shall explain their meaning by using the case of the single-inclusive jet transverse momentum p_T^{incl} (figs. 2 and 3) in order to be definite.

There are three panels in fig. 2. The upper one presents the absolute values of the three LO and the four NLO contributions to the cross section, as well as their sum; as

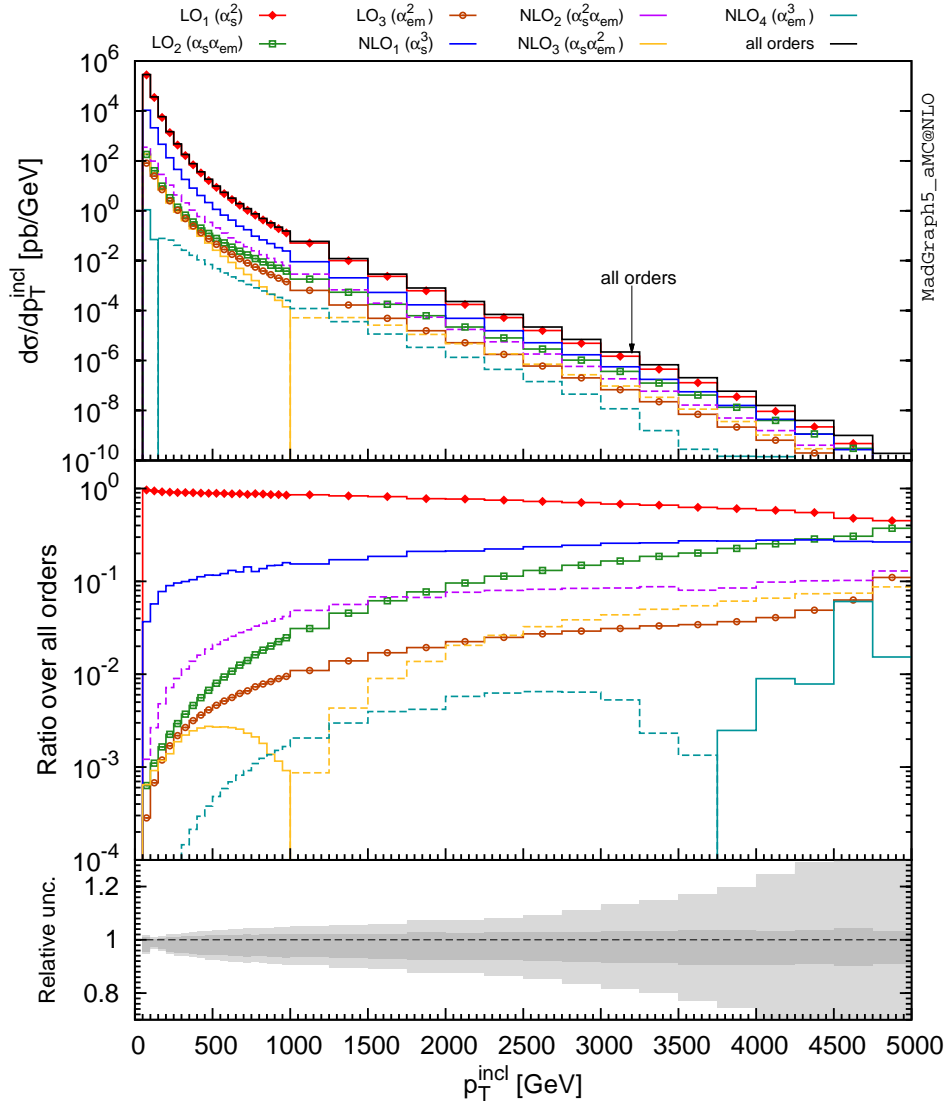


Figure 2. Single-inclusive transverse momentum.

was previously mentioned, a solid (dashed) pattern indicates that the corresponding result is positive (negative). The three LO results are displayed as histograms overlaid with symbols: red with full diamonds for Σ_{LO_1} , green with open boxes for Σ_{LO_2} , and brown with open circles for Σ_{LO_3} . The four NLO results are associated with plain histograms: blue for Σ_{NLO_1} , purple for Σ_{NLO_2} , yellow for Σ_{NLO_3} , and cyan for Σ_{NLO_4} ; the sum of all contributions is represented by the black histogram. The middle inset presents the ratios of the results shown in the upper inset, over the all-orders prediction; in other words, these are the fractional contributions of the Σ_{LO_i} and Σ_{NLO_i} terms to the most accurate result obtained from our simulations. The patterns employed in the middle inset are identical to those of the upper inset. Finally, the bottom inset presents the relative theoretical

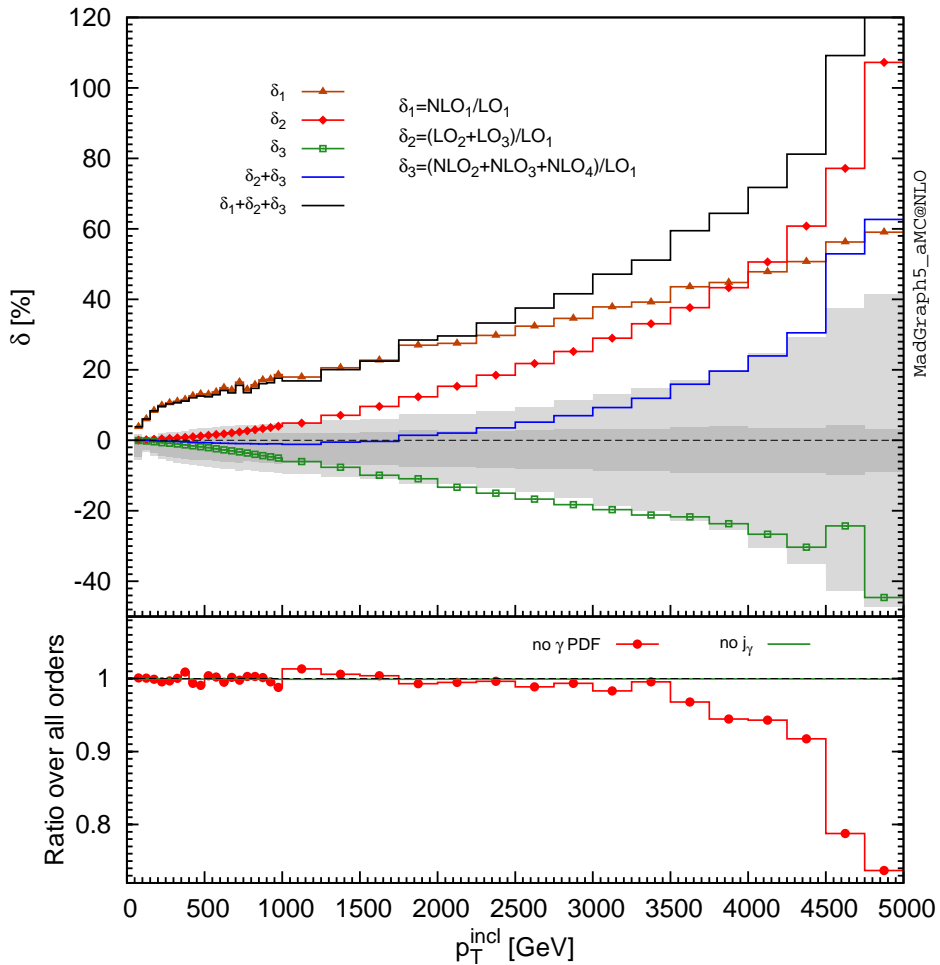


Figure 3. Single-inclusive transverse momentum.

uncertainty of the all-orders result, in two different ways: the light gray band corresponds to the hard-scale and PDF systematics (with the two summed linearly), while the dark gray band shows the hard-scale uncertainty only (see eq. (4.7) and thereabouts).

The main frame of fig. 3 presents various linear combinations of the results shown in fig. 2, in the form of ratios over the leading LO prediction, Σ_{LO_1} . In particular, we have defined the quantities:

$$\delta_1 = \frac{\Sigma_{NLO_1}}{\Sigma_{LO_1}}, \quad (4.12)$$

$$\delta_2 = \frac{\Sigma_{LO_2} + \Sigma_{LO_3}}{\Sigma_{LO_1}}, \quad (4.13)$$

$$\delta_3 = \frac{\Sigma_{NLO_2} + \Sigma_{NLO_3} + \Sigma_{NLO_4}}{\Sigma_{LO_1}}, \quad (4.14)$$

which are displayed as a brown histogram overlaid with full triangles (δ_1), a red histogram overlaid with full diamonds (δ_2), and a green histogram overlaid with open boxes (δ_3),

respectively. We also show the sum $\delta_2 + \delta_3$ as a blue histogram, and the sum $\delta_1 + \delta_2 + \delta_3$ as a black histogram. Finally, we report for reference the two uncertainty bands already shown in fig. 2. In view of the definition of Σ_{LO_i} and Σ_{NLO_i} , the physical meaning of the various curves presented in fig. 3 is the following. δ_1 is equal to $K_{\text{QCD}} - 1$, with K_{QCD} the K factor associated with a pure-QCD computation. δ_2 measures the relative impact of the two Born contributions which are non pure-QCD. δ_3 is equal to $K_{\text{QCD}} - 1$, with K_{QCD} the K factor associated with NLO contributions that are not pure QCD⁷. Thus, $\delta_1 + \delta_2 + \delta_3$ shows the effect on the best (i.e. the all-orders one) prediction of all contributions different from the dominant Born one (Σ_{LO_1}), while the comparison between δ_1 and $\delta_2 + \delta_3$ allows an immediate understanding of how much of that is due to either pure-QCD NLO corrections, or to other LO and NLO contributions.

The lower panel of fig. 3 displays two results, both of which are ratios of all-orders predictions obtained with specific conditions over the all-orders default prediction. The red histogram overlaid with full circles corresponds to setting to zero the photon PDF, while the green histogram corresponds to removing the photon-jet contributions.

The predictions for the single-inclusive jet transverse momentum shown in figs. 2 and 3 are dominated by the leading contributions at both the LO and the NLO for $p_T^{\text{incl}} \lesssim 2$ TeV. The impact of non-QCD contributions is essentially negligible up to those values, well within the scale uncertainty band. As is clear from fig. 3, specifically from the comparison of δ_2 , δ_3 , and $\delta_2 + \delta_3$, this is chiefly due to the very large cancellation that occurs between the LO_i and the NLO_i terms ($i \geq 2$) – note, from fig. 2, that this is not only true for the sums of such terms, but to some extent also for them individually, since the NLO ones are negative either in all or in a large part of the p_T range considered. Eventually, the LO cross sections grow faster in absolute value than their NLO counterparts. Thus, the sum of all results minus the leading LO term Σ_{LO_1} is indistinguishable from Σ_{NLO_1} up to 2 TeV, but then starts to differ significantly from it, to the extent that Σ_{NLO_1} contributes to less than 50% to the sum for those transverse momenta at the upper end of the range probed in our plots, $p_T^{\text{incl}} \gtrsim 4.5$ TeV. When one moves towards such large p_T^{incl} 's, one sees that the NLO scale uncertainty remains moderate, while that due to the PDFs grows rapidly, owing to the poor constraining power of the data currently used in PDF fits on the corresponding x region. To that PDF uncertainty, the photon contribution increases with p_T^{incl} (being equal to about 3% of the total PDF uncertainty at $p_T^{\text{incl}} \simeq 2.6$ TeV, and to about 22% at $p_T^{\text{incl}} \simeq 4.6$ TeV), but is never the dominant effect. From fig. 3 we see that the impact of the contributions that depend on the photon PDF is negligible for $p_T^{\text{incl}} \lesssim 3.5$ TeV, while it becomes substantial for larger values of the transverse momentum. Needless to say, the validity of this observation is restricted to the PDF used in the present simulations. The photon component in the NNPDF2.3QED set is mainly constrained by LHC Drell-Yan data via a reweighting procedure. This results in a significant photon density at large x that, however, is associated with a sizeable uncertainty. Other approaches, which rely either on assumptions on the functional form at some initial scale [66–68], or on a direct extraction

⁷As was already said, and for the sake of consistency, this K factor is defined by using the pure-QCD Born Σ_{LO_1} in the denominator.

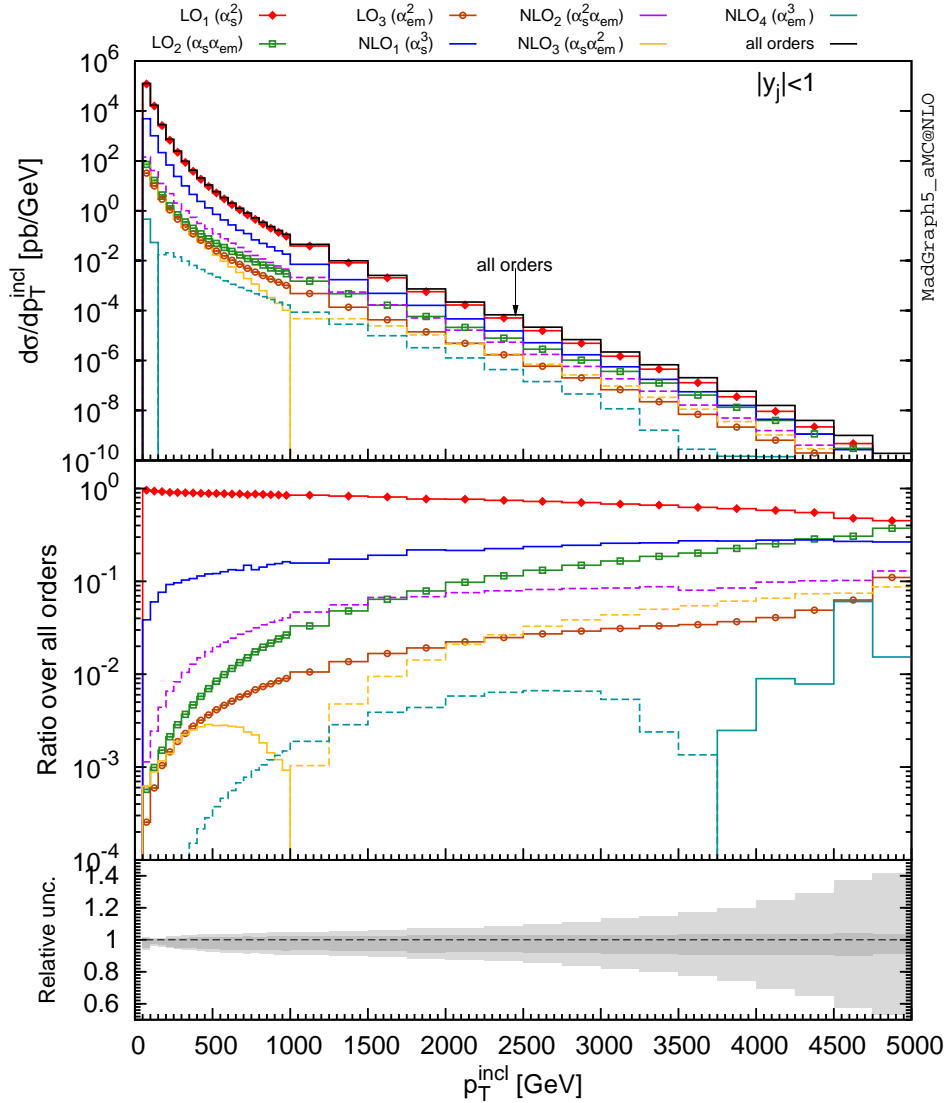


Figure 4. Single-inclusive transverse momentum, for $|y| \leq 1$.

from proton structure functions [69], suggest that its central value is much smaller than the NNPDF2.3 one at large x and rather precisely determined (in the recent sets), thus effectively lying close to the lower limit of the NNPDF2.3QED uncertainty band.

We also remark that the removal of the photon-jet cross sections has a negligible impact in the whole transverse momentum range considered. It does affect the individual LO_i and NLO_i , $i \geq 2$ contributions, especially LO_2 where it can be as large as 30%; however, this occurs mostly for $p_T^{\text{incl}} \lesssim 0.5$ TeV, where non-QCD terms can be safely ignored.

The single-inclusive transverse momentum is again shown in figs. 4 and 5, subject to the constraint $|y| \leq 1$ (in other words, each jet that gives a contribution to these histograms must satisfy a small-rapidity constraint). The patterns in these figures are very similar to

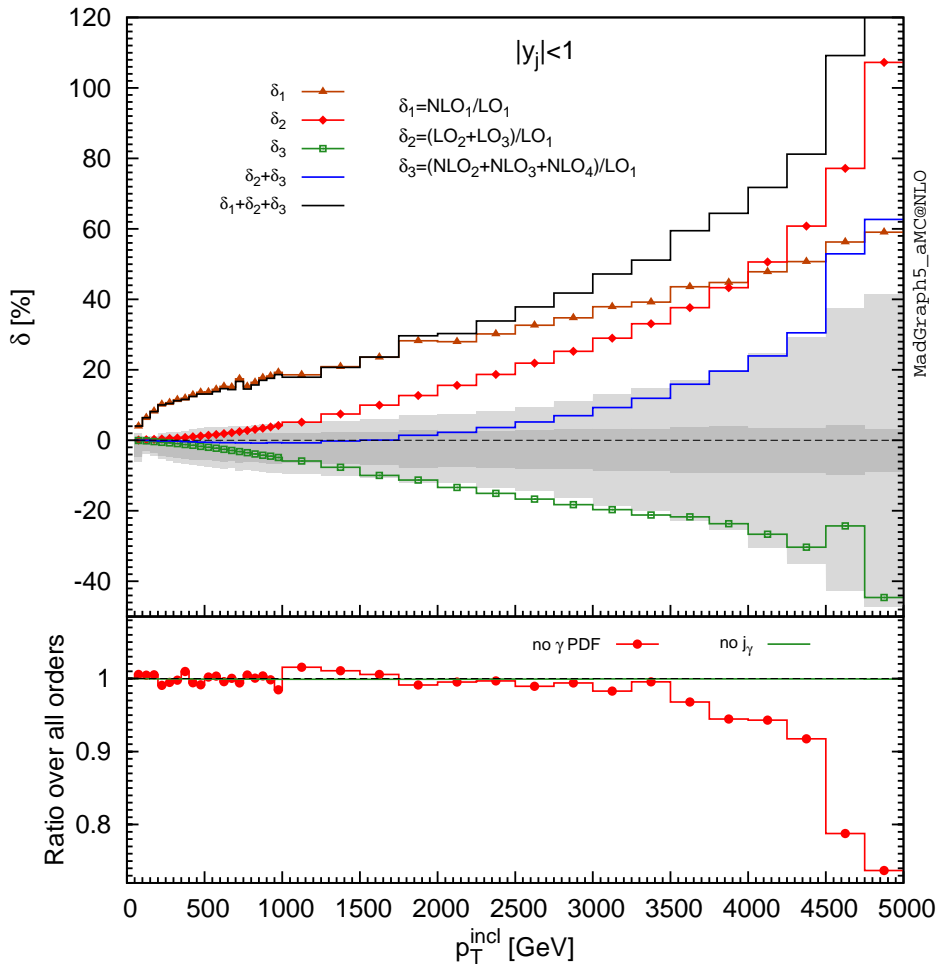


Figure 5. Single-inclusive transverse momentum, for $|y| \leq 1$.

those of figs. 2 and 3, respectively, owing to the dominance of central jets in the case inclusive over the whole rapidity range.

Things slightly change when one considers the rapidity intervals $1 < |y| \leq 2$ and $2 < |y| \leq 2.8$, whose cases are presented in figs. 6 and 7, and in figs. 8 and 9, respectively. In the transverse momentum region $p_T^{\text{incl}} \lesssim 1$ TeV, δ_2 tends to be marginally flatter when the rapidity is increased; conversely, δ_3 decreases, somehow more rapidly. The net effect is that the amount of cancellation between the LO and NLO cross sections is smaller the farther away one moves from central rapidities in this range of relatively small p_T^{incl} 's, so that the overall EW effects, that decrease the pure-QCD cross sections, are stronger the larger the rapidities. This is seen more clearly in fig. 10, where the results for δ_2 , δ_3 , and $\delta_2 + \delta_3$, already shown in figs. 5, 7, and 9, are presented together (as red, green, and blue histograms; the $|y| \leq 1$, $1 < |y| \leq 2$, and $2 < |y| \leq 2.8$ predictions are displayed as solid, dashed, and short-dashed histograms, respectively), by using a smaller y -axis scale w.r.t. those of the original plots. For larger transverse momenta the trend changes, with

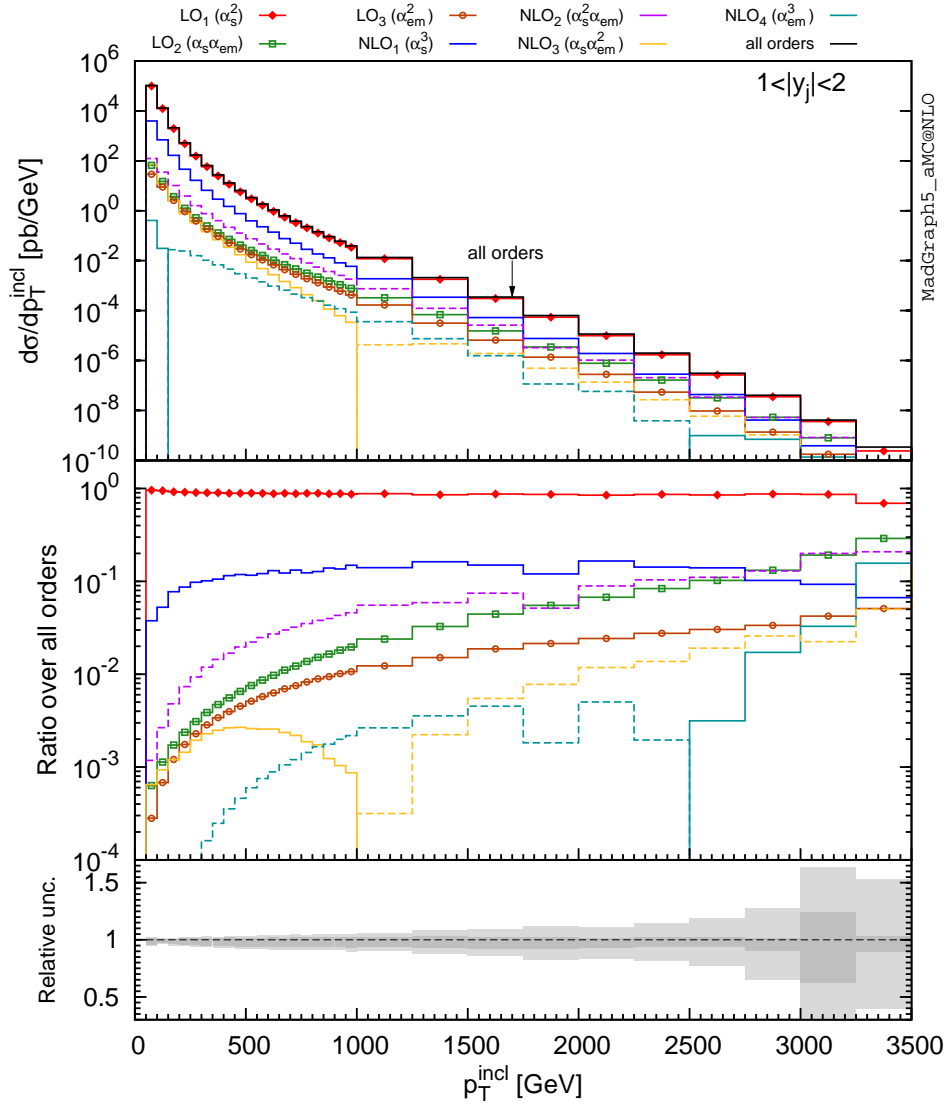


Figure 6. Single-inclusive transverse momentum, for $1 < |y| \leq 2$.

the positive LO contributions eventually becoming larger than their NLO counterparts (in absolute value). Thus, the $\delta_2 + \delta_3$ prediction crosses zero at $p_T^{\text{incl}} \sim 1.6$ TeV for $|y| \leq 1$, and at $p_T^{\text{incl}} \sim 2.5$ TeV for $1 < |y| \leq 2$ (the statistics is insufficient to draw any conclusion in the range $2 < |y| \leq 2.8$).

We conclude that, as far as the single-inclusive transverse momentum is concerned, the impact of LO and NLO contributions beyond the leading ones do depend on the rapidity range considered, and tends to decrease (increase) the pure-QCD results when moving away from the central region for small (large) p_T^{incl} ; in all cases, the absolute values of the overall effects are relatively small. This pattern is due to a variety of reasons; in particular, one may mention the fact that, the larger the rapidity, the more difficult it is to reach the

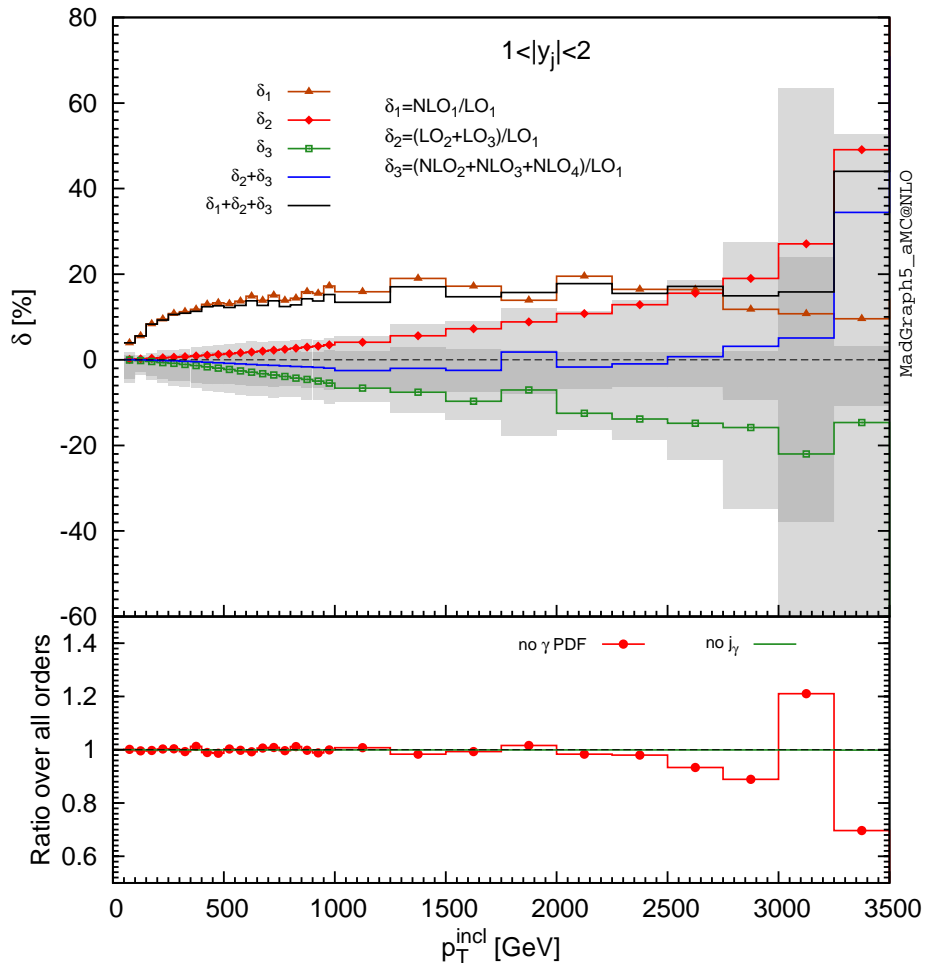


Figure 7. Single-inclusive transverse momentum, for $1 < |y| \leq 2$.

high- p_T region where EW effects are known to be more prominent, but also the fact that the extent of the cancellation between LO and NLO results is difficult to be predicted *a priori*. In any case, such a pattern must be taken into account in the context of PDF fits that aim to include EW corrections, and that need to consider different rapidity ranges in order to constrain more effectively the small- x region.

Our predictions for the invariant mass of the hardest-jet pair are given in figs. 11 and 12 (note that some of the histograms have been rescaled in the latter figure, in order to make them more clearly visible in the layout). NLO corrections are dominated by the pure-QCD ones Σ_{NLO_1} , that turn negative around $M_{12} \simeq 1$ TeV⁸. EW effects tend to decrease the cross section further, with the second-leading NLO corrections Σ_{NLO_2} being negative and larger in absolute value than the second-leading LO term Σ_{LO_2} . However, the overall impact on the physical cross section is rather small, and in particular smaller than

⁸There is a visible numerical instability that affects the large-mass predictions of Σ_{NLO_1} . It is due to significant cancellations between the real-emission and virtual contributions to that mass region.

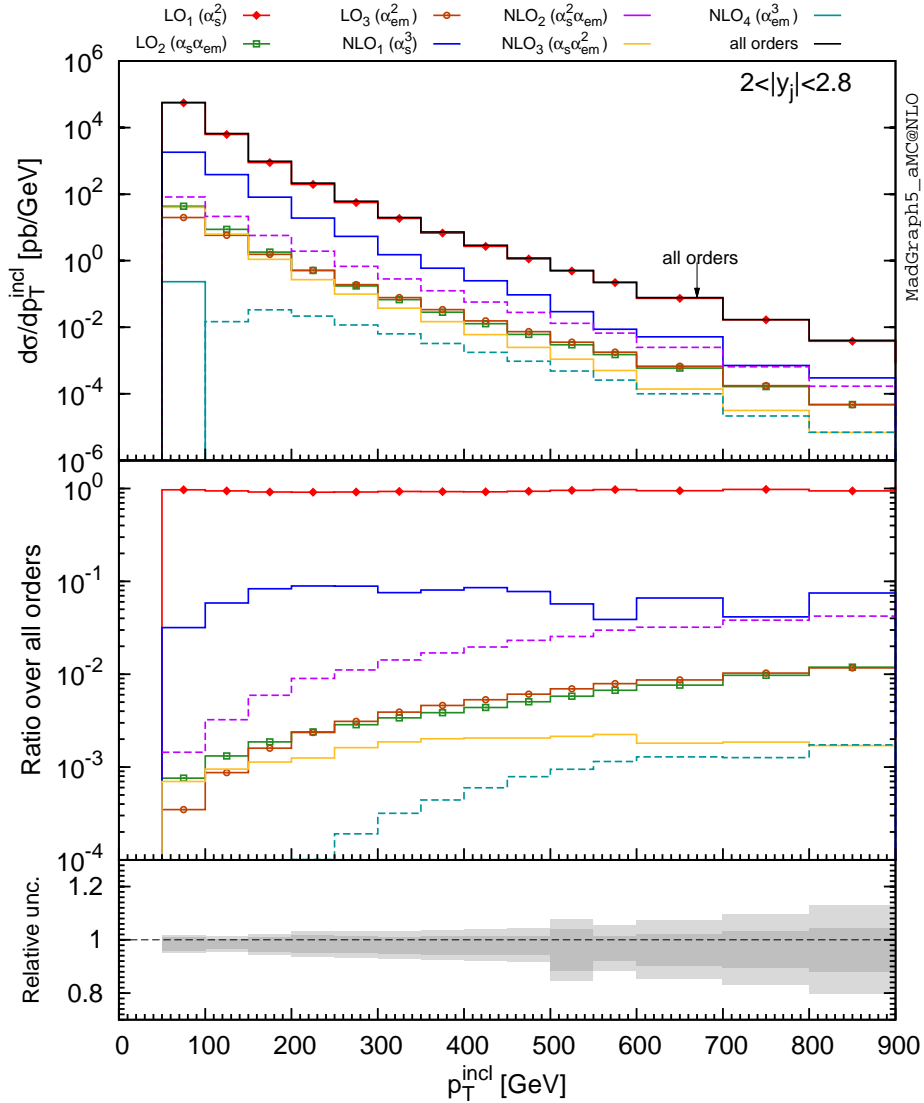


Figure 8. Single-inclusive transverse momentum, for $2 < |y| \leq 2.8$.

the hard-scale uncertainty. As was observed in ref. [10], even for mass values of several TeV's one is not fully in the Sudakov region, and thus EW contributions tend to follow the hierarchy established by the couplings, without major logarithmic enhancements. We also observe a very small impact of the removal of the photon jets. In this regard, the same comments as for the single-inclusive transverse momentum apply here. By removing photon-jet cross sections from Σ_{LO_2} , that term is halved at invariant masses smaller than 0.5 TeV; however, as can be seen from fig. 11, in that region its contribution to the all-orders rate is in practice negligible.

We finally show, in figs. 13 and 14, the rapidity separation between the two hardest jets (again, some of the histograms have been rescaled in the latter plot to improve its

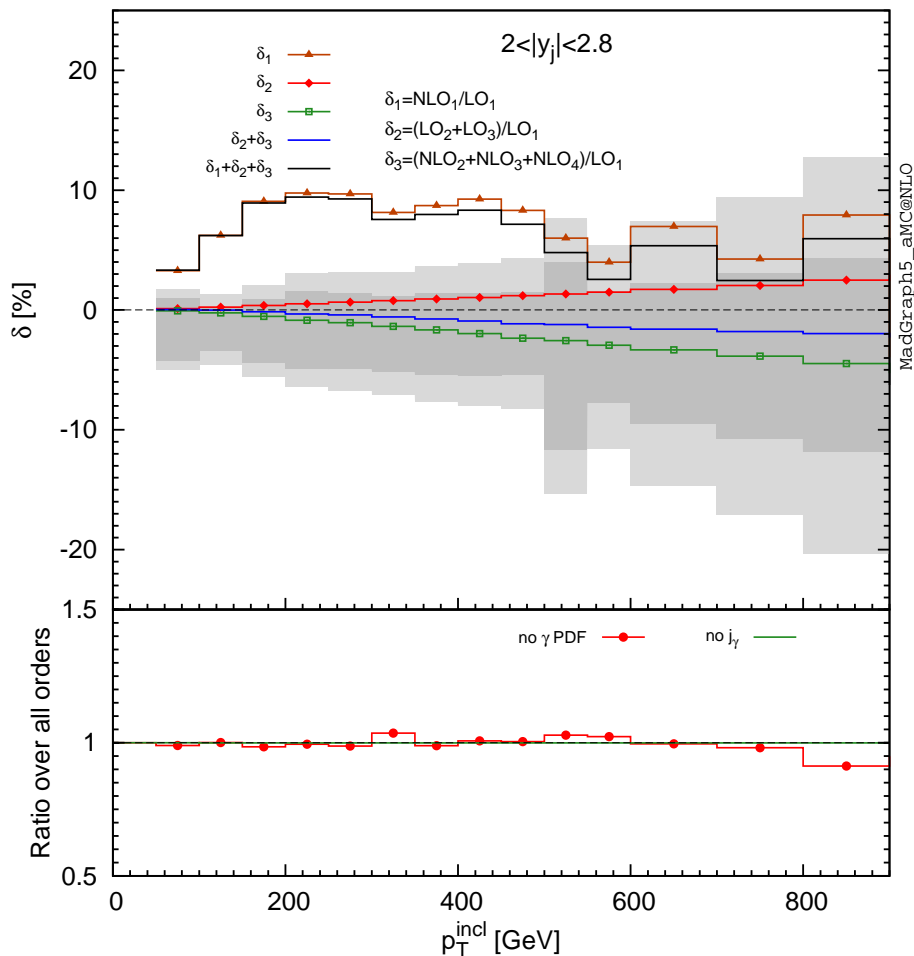


Figure 9. Single-inclusive transverse momentum, for $2 < |y| \leq 2.8$.

readability). This observable is dominated by low- p_T configurations, and as a consequence of that subleading terms, both at the LO and the NLO, are numerically extremely small, and completely swamped by hard-scale uncertainties. Leading NLO corrections are large, but almost flat in the whole range considered. As in the previous cases, the removal of photon jets is irrelevant to the all-orders result, while being important up to the largest rapidity separations in particular for Σ_{LO_2} .

5 Conclusions

In this paper we have studied the hadroproduction of dijets, and considered all of the LO and NLO contributions of QCD and EW origin to the corresponding cross section, presented as single-inclusive distributions and two-jet correlations for pp collisions at 13 TeV. By doing so, we have computed for the first time three subleading NLO corrections: the $\mathcal{O}(\alpha_s^2\alpha)$ electromagnetic one (our results include the contributions due to real-photon emissions), and the $\mathcal{O}(\alpha_s\alpha^2)$ and $\mathcal{O}(\alpha^3)$ EW ones. The calculations have been performed in

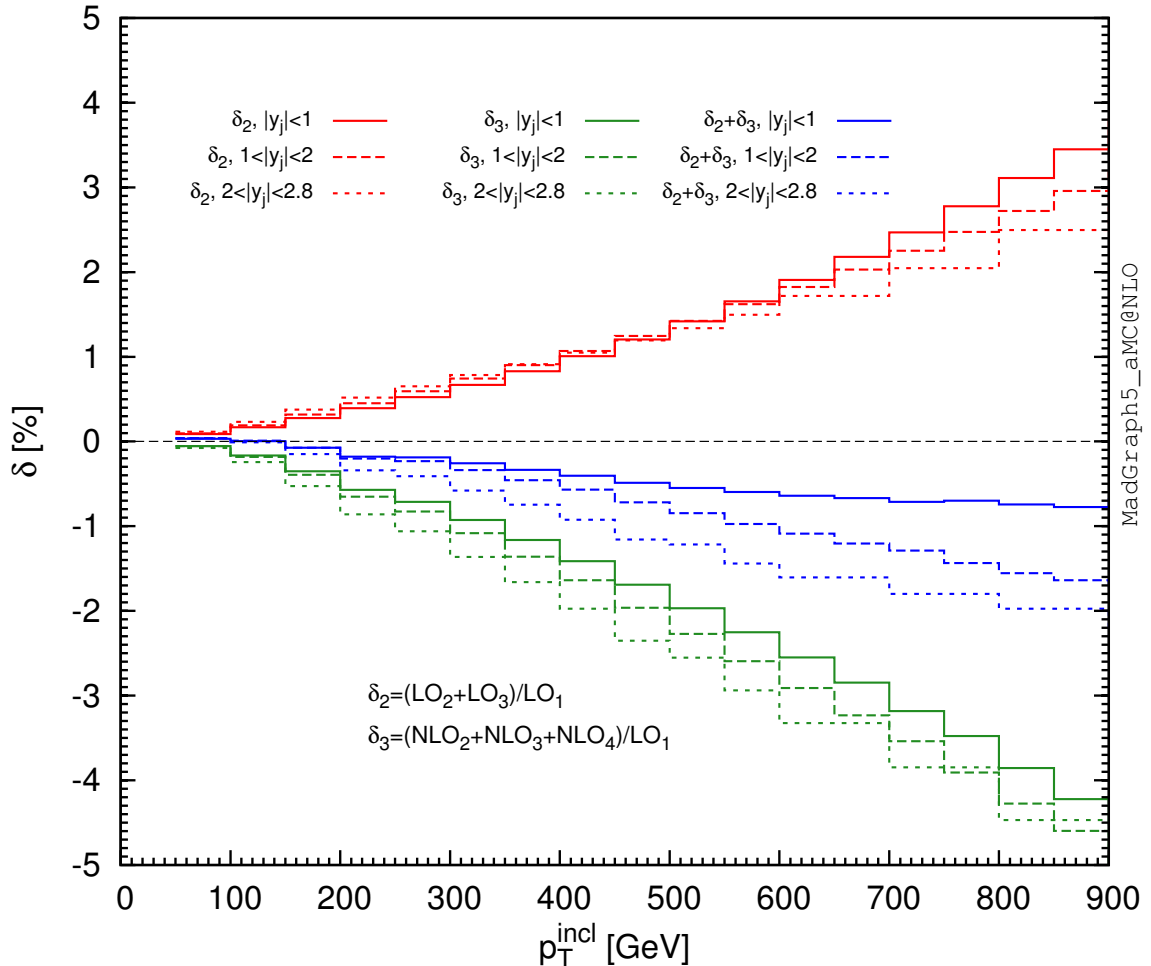


Figure 10. Single-inclusive transverse momentum; δ_2 and δ_3 predictions for the three rapidity regions already considered in figs. 5, 7, and 9.

the automated MADGRAPH5_AMC@NLO framework, which is thus extensively tested in a mixed-coupling scenario that features both EW and QCD loop corrections, and both QCD and QED real-emission subtractions.

When all subleading NLO corrections are computed, it is necessary to be particularly careful in the case one wants to not take into account jets that are predominantly of electromagnetic origin. Although from the phenomenological viewpoint we do not consider this operation to have a compelling motivation, we have outlined an IR-safe scheme through which this result can be achieved. Its exact implementation requires the use of fragmentation functions, whose determination from data is either poor or not available at present⁹. For the sake of this paper, we have adopted a more pragmatic strategy, which is a (perturbative) approximation of the more general scheme, that does not employ the fragmentation functions. We have shown that the removal of EW-dominated jets has a negligible impact at the level of observable differential rates, and one can thus safely work with democratic jets, in which all massless particles (quarks, gluons, photons, and leptons)

⁹However, the necessary ingredients for a technically-viable computation that leads to IR-finite cross sections can all be derived from purely perturbative information.

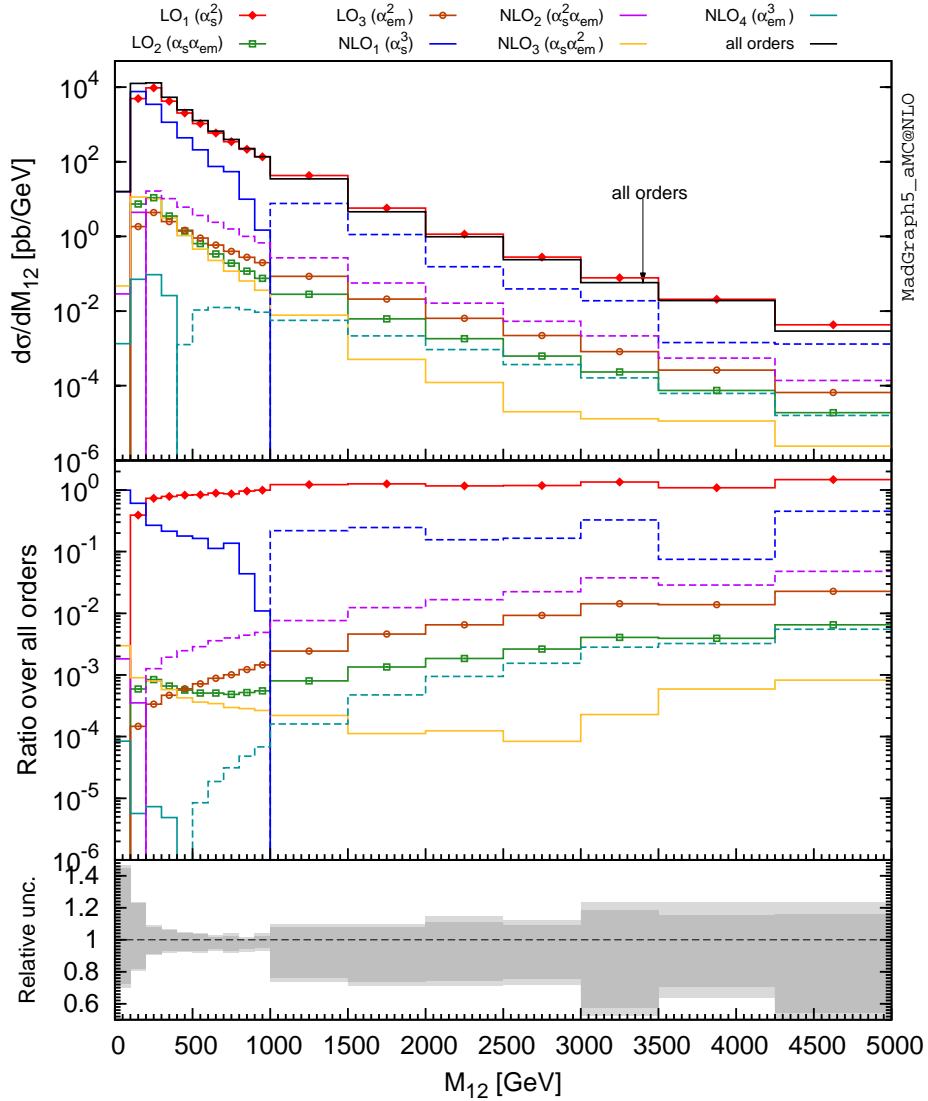


Figure 11. Invariant mass of the hardest jet pair.

are treated on equal footing.

In general, contributions that are expected to be subleading according to the coupling-constant combination they feature turn out to be indeed numerically subleading, with pure-QCD effects being dominant everywhere, except in the very-high transverse momentum region of the single-inclusive jet p_T . In other words, within the LO and NLO cross sections, we find that the hierarchy naively established on the basis of the couplings is largely respected, but we also remark that, in a significant fraction of the phase space, Σ_{NLO_2} is larger than Σ_{LO_2} . For all observables considered here, there are large cancellations between the LO and NLO subleading terms, which is one of the major motivations for computing them all in a consistent manner.

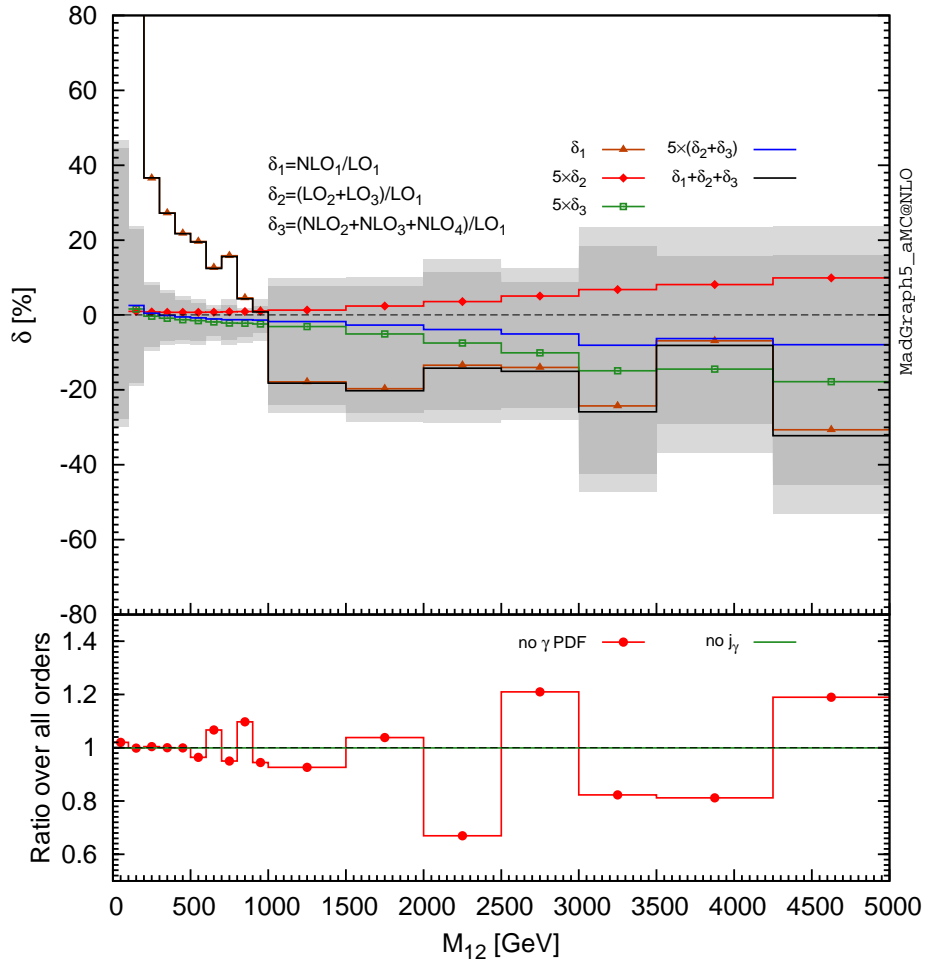


Figure 12. Invariant mass of the hardest jet pair.

Acknowledgements

This work is supported in part by the ERC grant 291377 “LHCtheory: Theoretical predictions and analyses of LHC physics: advancing the precision frontier”. SF thanks the CERN TH division for hospitality during the course of this work. SF is indebted to Stefano Catani for many stimulating discussions, and for comments on the manuscript; he is also grateful to Fabio Cossutti, Hannes Jung, Andrew Larkoski, and Wouter Waalewijn for comments on different aspects of their work. The work of MZ is supported by the European Union’s Horizon 2020 research and innovation programme under the Marie Skłodowska-Curie grant agreement No 660171 and in part by the ILP LABEX (ANR-10-LABX-63), in turn supported by French state funds managed by the ANR within the “Investissements d’Avenir” programme under reference ANR-11-IDEX-0004-02. RF and DP are supported by the Alexander von Humboldt Foundation in the framework of the Sofja Kovalevskaja Award Project “Event Simulation for the Large Hadron Collider at High Precision”. The work of

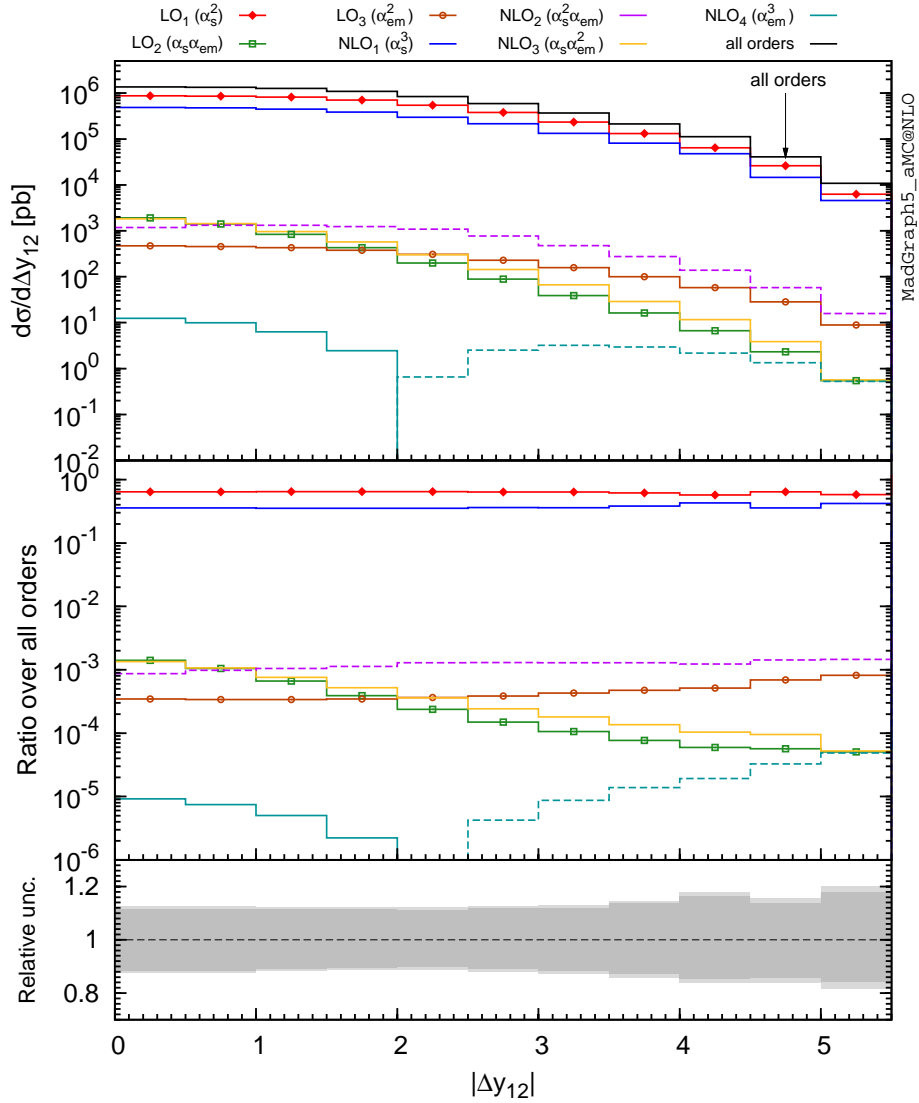


Figure 13. Rapidity distance between the two hardest jets.

VH is supported by the Swiss National Science Foundation (SNSF) with grant PBELP2 146525.

References

- [1] R. M. Harris and K. Kousouris, *Searches for Dijet Resonances at Hadron Colliders*, *Int. J. Mod. Phys. A* **26** (2011) 5005–5055, [[1110.5302](#)].
- [2] CDF collaboration, F. Abe et al., *Inclusive jet cross section in $\bar{p}p$ collisions at $\sqrt{s} = 1.8$ TeV*, *Phys. Rev. Lett.* **77** (1996) 438–443, [[hep-ex/9601008](#)].
- [3] S. D. Ellis, Z. Kunszt and D. E. Soper, *The One Jet Inclusive Cross-section at Order α_s^3 Quarks and Gluons*, *Phys. Rev. Lett.* **64** (1990) 2121.

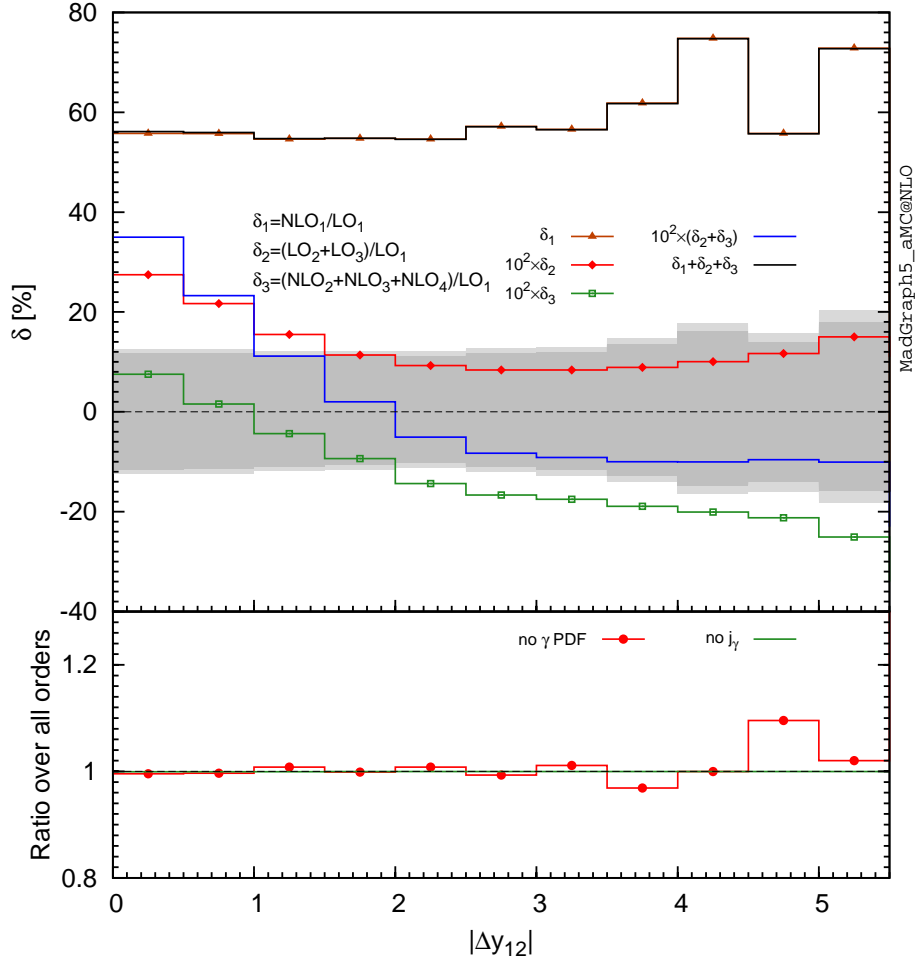


Figure 14. Rapidity distance between the two hardest jets.

- [4] F. Aversa, M. Greco, P. Chiappetta and J. P. Guillet, *Jet inclusive production to $\mathcal{O}(\alpha_s^3)$: Comparison with data*, *Phys. Rev. Lett.* **65** (1990) 401–403.
- [5] S. D. Ellis, Z. Kunszt and D. E. Soper, *Two jet production in hadron collisions at order α_s^3 in QCD*, *Phys. Rev. Lett.* **69** (1992) 1496–1499.
- [6] W. T. Giele, E. W. N. Glover and D. A. Kosower, *The Two-Jet Differential Cross Section at $\mathcal{O}(\alpha_s^3)$ in Hadron Collisions*, *Phys. Rev. Lett.* **73** (1994) 2019–2022, [[hep-ph/9403347](#)].
- [7] J. Currie, E. W. N. Glover and J. Pires, *NNLO QCD predictions for single jet inclusive production at the LHC*, [1611.01460](#).
- [8] A. Scharf, *Electroweak corrections to b-jet and di-jet production*, in *Particles and fields. Proceedings, Meeting of the Division of the American Physical Society, DPF 2009, Detroit, USA, July 26-31, 2009*, 2009. [0910.0223](#).
- [9] S. Moretti, M. R. Nolten and D. A. Ross, *Weak corrections to four-parton processes*, *Nucl. Phys.* **B759** (2006) 50–82, [[hep-ph/0606201](#)].
- [10] S. Dittmaier, A. Huss and C. Speckner, *Weak radiative corrections to dijet production at*

hadron colliders, *JHEP* **11** (2012) 095, [[1210.0438](#)].

- [11] P. Ciafaloni and D. Comelli, *Sudakov enhancement of electroweak corrections*, *Phys.Lett.* **B446** (1999) 278–284, [[hep-ph/9809321](#)].
- [12] M. Ciafaloni, P. Ciafaloni and D. Comelli, *Bloch-Nordsieck violating electroweak corrections to inclusive TeV scale hard processes*, *Phys.Rev.Lett.* **84** (2000) 4810–4813, [[hep-ph/0001142](#)].
- [13] A. Denner and S. Pozzorini, *One loop leading logarithms in electroweak radiative corrections. 1. Results*, *Eur.Phys.J.* **C18** (2001) 461–480, [[hep-ph/0010201](#)].
- [14] A. Denner and S. Pozzorini, *One loop leading logarithms in electroweak radiative corrections. 2. Factorization of collinear singularities*, *Eur.Phys.J.* **C21** (2001) 63–79, [[hep-ph/0104127](#)].
- [15] J. Alwall, R. Frederix, S. Frixione, V. Hirschi, F. Maltoni et al., *The automated computation of tree-level and next-to-leading order differential cross sections, and their matching to parton shower simulations*, *JHEP* **1407** (2014) 079, [[1405.0301](#)].
- [16] S. Frixione, V. Hirschi, D. Pagani, H. S. Shao and M. Zaro, *Electroweak and QCD corrections to top-pair hadroproduction in association with heavy bosons*, *JHEP* **06** (2015) 184, [[1504.03446](#)].
- [17] S. Frixione, V. Hirschi, D. Pagani, H. S. Shao and M. Zaro, *Weak corrections to Higgs hadroproduction in association with a top-quark pair*, *JHEP* **09** (2014) 065, [[1407.0823](#)].
- [18] S. Frixione, Z. Kunszt and A. Signer, *Three jet cross-sections to next-to-leading order*, *Nucl.Phys.* **B467** (1996) 399–442, [[hep-ph/9512328](#)].
- [19] S. Frixione, *A General approach to jet cross-sections in QCD*, *Nucl.Phys.* **B507** (1997) 295–314, [[hep-ph/9706545](#)].
- [20] R. Frederix, S. Frixione, F. Maltoni and T. Stelzer, *Automation of next-to-leading order computations in QCD: The FKS subtraction*, *JHEP* **0910** (2009) 003, [[0908.4272](#)].
- [21] R. Frederix, S. Frixione, A. S. Papanastasiou, S. Prestel and P. Torrielli, *Off-shell single-top production at NLO matched to parton showers*, *JHEP* **06** (2016) 027, [[1603.01178](#)].
- [22] G. Ossola, C. G. Papadopoulos and R. Pittau, *Reducing full one-loop amplitudes to scalar integrals at the integrand level*, *Nucl.Phys.* **B763** (2007) 147–169, [[hep-ph/0609007](#)].
- [23] P. Mastrolia, E. Mirabella and T. Peraro, *Integrand reduction of one-loop scattering amplitudes through Laurent series expansion*, *JHEP* **06** (2012) 095, [[1203.0291](#)].
- [24] G. Passarino and M. Veltman, *One Loop Corrections for e^+e^- Annihilation Into $\mu^+\mu^-$ in the Weinberg Model*, *Nucl.Phys.* **B160** (1979) 151.
- [25] A. I. Davydychev, *A Simple formula for reducing Feynman diagrams to scalar integrals*, *Phys.Lett.* **B263** (1991) 107–111.
- [26] A. Denner and S. Dittmaier, *Reduction schemes for one-loop tensor integrals*, *Nucl. Phys.* **B734** (2006) 62–115, [[hep-ph/0509141](#)].
- [27] V. Hirschi, R. Frederix, S. Frixione, M. V. Garzelli, F. Maltoni et al., *Automation of one-loop QCD corrections*, *JHEP* **1105** (2011) 044, [[1103.0621](#)].
- [28] G. Ossola, C. G. Papadopoulos and R. Pittau, *CutTools: A Program implementing the OPP reduction method to compute one-loop amplitudes*, *JHEP* **0803** (2008) 042, [[0711.3596](#)].

- [29] T. Peraro, *Ninja: Automated Integrand Reduction via Laurent Expansion for One-Loop Amplitudes*, *Comput. Phys. Commun.* **185** (2014) 2771–2797, [[1403.1229](#)].
- [30] V. Hirschi and T. Peraro, *Tensor integrand reduction via Laurent expansion*, *JHEP* **06** (2016) 060, [[1604.01363](#)].
- [31] H.-S. Shao, *Iregi user manual*, unpublished, .
- [32] F. Cascioli, P. Maierhofer and S. Pozzorini, *Scattering Amplitudes with Open Loops*, *Phys.Rev.Lett.* **108** (2012) 111601, [[1111.5206](#)].
- [33] E. W. N. Glover and A. G. Morgan, *Measuring the photon fragmentation function at LEP*, *Z. Phys.* **C62** (1994) 311–322.
- [34] CMS collaboration, V. Khachatryan et al., *Measurement of the inclusive 3-jet production differential cross section in proton-proton collisions at 7 TeV and determination of the strong coupling constant in the TeV range*, *Eur. Phys. J.* **C75** (2015) 186, [[1412.1633](#)].
- [35] CMS collaboration, V. Khachatryan et al., *Measurement of the double-differential inclusive jet cross section in proton-proton collisions at $\sqrt{s} = 13$ TeV*, *Eur. Phys. J.* **C76** (2016) 451, [[1605.04436](#)].
- [36] ATLAS collaboration, G. Aad et al., *Measurement of four-jet differential cross sections in $\sqrt{s} = 8$ TeV proton-proton collisions using the ATLAS detector*, *JHEP* **12** (2015) 105, [[1509.07335](#)].
- [37] CMS collaboration, V. Khachatryan et al., *Measurement and QCD analysis of double-differential inclusive jet cross-sections in pp collisions at $\sqrt{s} = 8$ TeV and ratios to 2.76 and 7 TeV*, [1609.05331](#).
- [38] CMS collaboration, V. Khachatryan et al., *Measurement of dijet azimuthal decorrelation in pp collisions at $\sqrt{s} = 8$ TeV*, *Eur. Phys. J.* **C76** (2016) 536, [[1602.04384](#)].
- [39] CMS collaboration, V. Khachatryan et al., *Measurement of the inclusive jet cross section in pp collisions at $\sqrt{s} = 2.76$ TeV*, *Eur. Phys. J.* **C76** (2016) 265, [[1512.06212](#)].
- [40] CMS collaboration, S. Chatrchyan et al., *Measurement of the ratio of inclusive jet cross sections using the anti- k_T algorithm with radius parameters $R=0.5$ and 0.7 in pp collisions at $\sqrt{s} = 7$ TeV*, *Phys. Rev.* **D90** (2014) 072006, [[1406.0324](#)].
- [41] CMS collaboration, V. Khachatryan et al., *Study of hadronic event-shape variables in multijet final states in pp collisions at $\sqrt{s} = 7$ TeV*, *JHEP* **10** (2014) 87, [[1407.2856](#)].
- [42] CMS collaboration, S. Chatrchyan et al., *Measurements of differential jet cross sections in proton-proton collisions at $\sqrt{s} = 7$ TeV with the CMS detector*, *Phys. Rev.* **D87** (2013) 112002, [[1212.6660](#)].
- [43] ATLAS collaboration, G. Aad et al., *Measurement of three-jet production cross-sections in pp collisions at 7 TeV centre-of-mass energy using the ATLAS detector*, *Eur. Phys. J.* **C75** (2015) 228, [[1411.1855](#)].
- [44] ATLAS collaboration, G. Aad et al., *Measurement of the inclusive jet cross-section in proton-proton collisions at $\sqrt{s} = 7$ TeV using 4.5 fb^{-1} of data with the ATLAS detector*, *JHEP* **02** (2015) 153, [[1410.8857](#)].
- [45] ATLAS collaboration, G. Aad et al., *Measurement of dijet cross sections in pp collisions at 7 TeV centre-of-mass energy using the ATLAS detector*, *JHEP* **05** (2014) 059, [[1312.3524](#)].

- [46] ATLAS collaboration, G. Aad et al., *Measurement of inclusive jet and dijet production in pp collisions at $\sqrt{s} = 7$ TeV using the ATLAS detector*, *Phys. Rev.* **D86** (2012) 014022, [[1112.6297](#)].
- [47] A. Denner, S. Dittmaier, T. Kasprzik and A. Muck, *Electroweak corrections to $W + jet$ hadroproduction including leptonic W -boson decays*, *JHEP* **08** (2009) 075, [[0906.1656](#)].
- [48] A. Denner, L. Hofer, A. Scharf and S. Uccirati, *Electroweak corrections to lepton pair production in association with two hard jets at the LHC*, *JHEP* **01** (2015) 094, [[1411.0916](#)].
- [49] S. Kallweit, J. M. Lindert, P. Maierhofer, S. Pozzorini and M. Schnherr, *NLO electroweak automation and precise predictions for W +multijet production at the LHC*, *JHEP* **04** (2015) 012, [[1412.5157](#)].
- [50] M. Chiesa, N. Greiner and F. Tramontano, *Automation of electroweak corrections for LHC processes*, *J. Phys.* **G43** (2016) 013002, [[1507.08579](#)].
- [51] S. Catani and S. Frixione, *in preparation*, .
- [52] S. Dittmaier, A. Kabelschacht and T. Kasprzik, *Polarized QED splittings of massive fermions and dipole subtraction for non-collinear-safe observables*, *Nucl. Phys.* **B800** (2008) 146–189, [[0802.1405](#)].
- [53] A. Denner, *Techniques for calculation of electroweak radiative corrections at the one loop level and results for W physics at LEP-200*, *Fortsch. Phys.* **41** (1993) 307–420, [[0709.1075](#)].
- [54] S. Frixione, *Isolated photons in perturbative QCD*, *Phys. Lett.* **B429** (1998) 369–374, [[hep-ph/9801442](#)].
- [55] S. Catani, Y. L. Dokshitzer, M. H. Seymour and B. R. Webber, *Longitudinally invariant K_t clustering algorithms for hadron hadron collisions*, *Nucl. Phys.* **B406** (1993) 187–224.
- [56] M. Cacciari, G. P. Salam and G. Soyez, *FastJet User Manual*, *Eur.Phys.J.* **C72** (2012) 1896, [[1111.6097](#)].
- [57] A. Denner, S. Dittmaier, M. Roth and D. Wackerroth, *Predictions for all processes $e+ e- \rightarrow 4$ fermions + gamma*, *Nucl. Phys.* **B560** (1999) 33–65, [[hep-ph/9904472](#)].
- [58] A. Denner, S. Dittmaier, M. Roth and L. H. Wieders, *Electroweak corrections to charged-current $e+ e- \rightarrow 4$ fermion processes: Technical details and further results*, *Nucl. Phys.* **B724** (2005) 247–294, [[hep-ph/0505042](#)].
- [59] NNPDF collaboration, R. D. Ball et al., *Parton distributions with QED corrections*, *Nucl.Phys.* **B877** (2013) 290–320, [[1308.0598](#)].
- [60] A. Buckley, J. Ferrando, S. Lloyd, K. Nordström, B. Page, M. Rfenacht et al., *LHAPDF6: parton density access in the LHC precision era*, *Eur. Phys. J.* **C75** (2015) 132, [[1412.7420](#)].
- [61] R. Frederix, S. Frixione, V. Hirschi, F. Maltoni, R. Pittau et al., *Four-lepton production at hadron colliders: aMC@NLO predictions with theoretical uncertainties*, *JHEP* **1202** (2012) 099, [[1110.4738](#)].
- [62] NNPDF COLLABORATION collaboration, R. D. Ball et al., *A Determination of parton distributions with faithful uncertainty estimation*, *Nucl.Phys.* **B809** (2009) 1–63, [[0808.1231](#)].
- [63] M. Cacciari, M. Greco and P. Nason, *The $P(T)$ spectrum in heavy flavor hadroproduction*, *JHEP* **05** (1998) 007, [[hep-ph/9803400](#)].

- [64] J. R. Andersen et al., *Les Houches 2015: Physics at TeV Colliders Standard Model Working Group Report*, in *9th Les Houches Workshop on Physics at TeV Colliders (PhysTeV 2015) Les Houches, France, June 1-19, 2015*, 2016. [1605.04692](#).
- [65] S. Frixione and G. Ridolfi, *Jet photoproduction at HERA*, *Nucl. Phys.* **B507** (1997) 315–333, [[hep-ph/9707345](#)].
- [66] C. Schmidt, J. Pumplin, D. Stump and C. P. Yuan, *CT14QED parton distribution functions from isolated photon production in deep inelastic scattering*, *Phys. Rev.* **D93** (2016) 114015, [[1509.02905](#)].
- [67] L. A. Harland-Lang, V. A. Khoze and M. G. Ryskin, *Photon-initiated processes at high mass*, *Phys. Rev.* **D94** (2016) 074008, [[1607.04635](#)].
- [68] A. D. Martin, R. G. Roberts, W. J. Stirling and R. S. Thorne, *Parton distributions incorporating QED contributions*, *Eur. Phys. J.* **C39** (2005) 155–161, [[hep-ph/0411040](#)].
- [69] A. Manohar, P. Nason, G. P. Salam and G. Zanderighi, *How bright is the proton? A precise determination of the photon PDF*, [1607.04266](#).